



HAL
open science

Monitoring Deep Sea Currents With Seafloor Distributed Acoustic Sensing

Daniel Mata, Anthony Sladen, Jean-paul Ampuero, E. Diego Mercerat, Diane Rivet

► **To cite this version:**

Daniel Mata, Anthony Sladen, Jean-paul Ampuero, E. Diego Mercerat, Diane Rivet. Monitoring Deep Sea Currents With Seafloor Distributed Acoustic Sensing. *Earth and Space Science*, 2023, 10 (6), 10.1029/2022EA002723 . insu-04155250

HAL Id: insu-04155250

<https://insu.hal.science/insu-04155250>

Submitted on 7 Jul 2023

HAL is a multi-disciplinary open access archive for the deposit and dissemination of scientific research documents, whether they are published or not. The documents may come from teaching and research institutions in France or abroad, or from public or private research centers.

L'archive ouverte pluridisciplinaire **HAL**, est destinée au dépôt et à la diffusion de documents scientifiques de niveau recherche, publiés ou non, émanant des établissements d'enseignement et de recherche français ou étrangers, des laboratoires publics ou privés.



Distributed under a Creative Commons Attribution - NonCommercial - NoDerivatives 4.0
International License

Earth and Space Science



RESEARCH ARTICLE

10.1029/2022EA002723

Monitoring Deep Sea Currents With Seafloor Distributed Acoustic Sensing

Daniel Mata Flores¹ , Anthony Sladen¹, Jean-Paul Ampuero¹ , E. Diego Mercerat², and Diane Rivet¹ 

¹Université Côte d'Azur, CNRS, Observatoire de la Côte d'Azur, IRD, Géoazur, Valbonne, France, ²CEREMA Méditerranée, Valbonne, France

Key Points:

- Sections of seafloor fiber cables feature oscillations driven by ocean currents that are observable with distributed acoustic sensing (DAS)
- Cable oscillation frequencies provide ocean current speed time series through the Strouhal number relation of vortex-induced vibrations
- Spectral analysis of DAS-derived ocean current time series provides valuable information on oceanic internal gravity waves

Supporting Information:

Supporting Information may be found in the online version of this article.

Correspondence to:

D. Mata Flores,
daniel.e.mata.f@gmail.com

Citation:

Mata Flores, D., Sladen, A., Ampuero, J.-P., Mercerat, E. D., & Rivet, D. (2023). Monitoring deep Sea currents with seafloor distributed acoustic sensing. *Earth and Space Science*, 10, e2022EA002723. <https://doi.org/10.1029/2022EA002723>

Received 7 NOV 2022
Accepted 25 MAY 2023

Author Contributions:

Conceptualization: Daniel Mata Flores, Anthony Sladen, Jean-Paul Ampuero, E. Diego Mercerat, Diane Rivet

Formal analysis: Daniel Mata Flores, Jean-Paul Ampuero

Funding acquisition: Anthony Sladen

Investigation: Daniel Mata Flores, E. Diego Mercerat

Methodology: Daniel Mata Flores, Anthony Sladen, Jean-Paul Ampuero, E. Diego Mercerat, Diane Rivet

Project Administration: Anthony Sladen

Supervision: Anthony Sladen, Jean-Paul Ampuero

© 2023 The Authors.

This is an open access article under the terms of the [Creative Commons Attribution-NonCommercial License](https://creativecommons.org/licenses/by-nc/4.0/), which permits use, distribution and reproduction in any medium, provided the original work is properly cited and is not used for commercial purposes.

Abstract Underwater fiber optic cables commonly traverse a variety of seafloor conditions, which leads to an uneven mechanical coupling between the cable and the ocean bottom. On rough seafloor bathymetry, some cable portions might be suspended and thus susceptible to vortex-induced vibrations (VIV) driven by deep ocean currents. Here, we examine the potential of distributed acoustic sensing (DAS) to monitor deep-sea currents along suspended sections of underwater telecom fiber optic cables undergoing VIV. Oscillations of a seafloor fiber optic cable located in southern France are recorded by DAS along cable sections presumably hanging. Their characteristic frequencies are lower than 1 Hz, at different ocean depths, and have an amplitude-dependency consistent with the driving mechanism being VIV. Based on a theoretical proportionality between current speed and VIV frequencies, we derive ocean current speed time series at 2,390 m depth from the vortex shedding frequencies recorded by DAS. The DAS-derived current speed time series is in agreement with recordings by a current meter located 3.75 km away from the hanging cable section (similar dominant period, high correlation after time shift). The DAS-derived current speed time series displays features, such as characteristic periods and spectral decay, associated with the generation of internal gravity waves and weak oceanic turbulence in the Mediterranean Sea. The results demonstrate the potential of DAS along hanging segments of fiber optic cables to monitor a wide range of oceanography processes, at depths barely studied with current instrumentation.

Plain Language Summary Ocean current speed recordings are rare below 1,500 m depth due to the cost of instrumentation in deep ocean environments. In this study, we demonstrate that deep-sea current speeds can be obtained using measurements of deformation along suspended sections of seafloor fiber optic cables by a technique called distributed acoustic sensing (DAS). As ocean currents hit hanging cable segments, they generate vortex that shed off from the cable at a frequency called “vortex shedding frequency.” We show field evidence that the resulting cable oscillations can be recorded by seafloor DAS. We infer ocean current speed time series from the vortex shedding frequencies recorded by DAS across a hanging section of an underwater fiber optic cable in southern France. The DAS-derived time series is in agreement with the one recorded by a nearby current meter. Our results demonstrate the potential of DAS to monitor the generation of internal gravity waves in the Mediterranean Sea at depths barely studied with the current instrumentation, and suggest that the technique presented here to estimate seafloor current speeds may be used for investigating several processes in oceanography.

1. Introduction

Understanding ocean circulation is crucial for climate change modeling. Oceans play a determinant role in the climate system: they contain Earth's dominant reservoirs of heat and freshwater in near equilibrium with the atmosphere and cryosphere, and can trigger and non-linearly amplify climate change via multiple mechanisms (Rahmstorf, 2002; Semtner, 1995; Wunsch, 2016). In addition, ocean currents are one of the main sources of turbulent energy contributing to mix the ocean and controlling the sediment distribution of marine deposits (Bryden et al., 2012; Munk & Wunsch, 1998). Yet, observations of ocean currents are rare, especially in deep seafloor environments, due to the cost of instrumentation. The scarcity of deep ocean current data leads to incomplete observational time series of ocean dynamics, which hinders the establishment of long-term trends of ocean circulation (Rahmstorf, 2002). Moorings and gliders are a first good approach to fill the data gap but their energy and cost budgets hold back the deployment of additional sensors (Bryden et al., 2012). The Argo program floats have been expanding the coverage of deep oceanographic data, but they are limited to a profiling depth of

Validation: Anthony Sladen, Jean-Paul Ampuero

Writing – original draft: Daniel Mata Flores, Jean-Paul Ampuero

Writing – review & editing: Anthony Sladen, Jean-Paul Ampuero, E. Diego Mercerat, Diane Rivet

approximately 2,000 m, leaving half of the deep ocean unsampled (Bryden et al., 2012). Moreover, the combination of ships-of-opportunity and float dispersion is not sufficient to sample regions of the globe with difficult access (Roemmich et al., 2009).

Underwater telecommunication cables, the only infrastructure already crisscrossing the ocean floors, could be leveraged to enhance ocean monitoring. The SMART (Science Monitoring And Reliable Telecommunications) initiative has proposed to constrain ocean circulation by temperature sensors integrated into the repeaters of undersea telecommunication cables (Howe et al., 2019), but it does not address the recording of ocean currents. Analysis of the state of polarization (SOP) of regular optical telecommunication channels can be used to monitor ocean swells produced by distant storms (Zhan et al., 2021) but has two main limitations: the low signal-to-noise ratio of the interferometry and its very coarse spatial resolution, as the measurement is integrated over the whole cable length. Long-distance optical interferometry across transoceanic cables has been proposed to monitor tidal currents (Marra et al., 2022), but would also have limited spatial resolution of several tens of km, the distance between cable repeaters. Among the different photonics-based metrology techniques, distributed acoustic sensing (DAS) has been rapidly and widely adopted, with demonstration of a large potential of applications in physical oceanography (Lindsey et al., 2019; Sladen et al., 2019; Williams et al., 2022). DAS probes changes in the Rayleigh back-scattering pattern along tens of kilometers of fiber optic cables, effectively turning cables into arrays of thousands of strain sensors (Hartog, 2017). DAS typically records nano variations of strains, enabling the detection of a wide range of processes. Underwater cables are interrogated by DAS from their on-shore termination points, which may allow uninterrupted monitoring of the ocean dynamics from land.

Underwater fiber cables commonly traverse a variety of seafloor conditions, which leads to an uneven mechanical coupling between the cable and the ocean bottom. On rough seafloor bathymetry, some cable portions might be suspended and thus susceptible to vortex-induced vibrations (VIV) driven by deep ocean currents. Along slender objects exposed to water currents, VIV manifests as high-amplitude oscillations with characteristic frequencies associated to the periodicity of vortex shedding. The phenomenon has been previously reported at scales ranging from deep-water oil and gas facilities, such as risers, to Ocean Bottom Seismometers (OBS) antennas (Duennebier et al., 1981; Hong & Shah, 2018; Stähler et al., 2018; Trim et al., 2005). The relation between DAS, VIV, and ocean currents has been previously cited (Sladen et al., 2019) but, to the best of our knowledge, no quantitative link has been established in preceding works. We report here observations of VIV along a seafloor fiber cable monitored with DAS in the Mediterranean Sea, for which independent measurements of ocean currents at the sea bottom are available as validation data.

Here, we examine the potential of DAS to monitor deep-sea currents, using the fundamental frequency of quasi-harmonic oscillations recorded along sections of an underwater telecommunication cable located in southern France. We first identify cable segments featuring the oscillations, which we interpret as cable portions suspended and exposed to VIV. Using VIV theory, we convert the cable oscillation frequencies into an ocean current speed time series. We further show that DAS-derived current speeds are comparable to speeds recorded by a current meter deployed 3.75 km away, also on the deep seafloor. The spectral content of the DAS-derived time series offers insight into oceanographic processes involving ocean circulation and stratification in the Mediterranean Sea.

2. Data Overview

The electro-optic cable monitored in this study is located offshore Toulon, south of France (Figure 1a). It is part of the MEUST-NUMerEnv project (Mediterranean Eurocentre for Underwater Sciences and Technologies-Neutrino Mer Environnement) (Lamare, 2016) and is used to transmit the data acquired at its underwater end by the KM3NeT/ORCA (Oscillation Research with Cosmics in the Abyss) neutrino detector (Coyle & KM3NeT Collaboration, 2017). The cable trajectory slightly differs from the one described in Sladen et al. (2019) due to maintenance works performed in October 2018, which involved the replacement of the distant half of the cable. All cable sections analyzed here are from this replaced part of the cable which traverses different oceanic features, from the continental slope to the abyssal plain, that may allow hanging sections (Figure 1b). According to technical specifications provided during the maintenance works, the diameter of the cable segments presented here is 2.75 cm.

DAS strain data (strain parallel to the cable axis) were collected from 11 July to 31 July 2019, using an Aragon Photonics HDAS interrogator that relies on chirped pulse ϕ -OTDR. Distributed Raman amplification was used

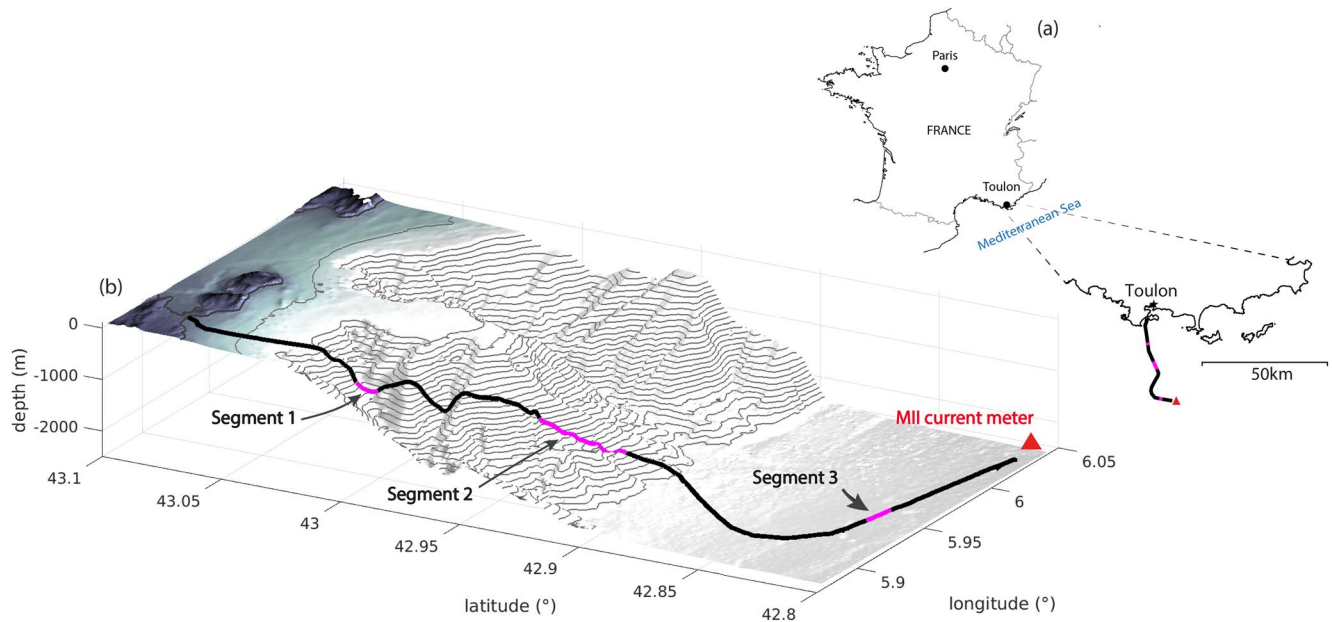


Figure 1. Location and bathymetry model of the underwater Mediterranean Eurocentre for Underwater Sciences and Technologies cable. The optic fiber cable depicted in (a) offshore Toulon, France, traverses different seafloor features throughout its 44.8-km length (b). Nine hanging sections were identified along three segments of the cable trajectory (1 in Segment 1, 6 in Segment 2 and 2 in Segment 3). The red triangle represents the position of an Acoustic Doppler Current Profiler (*MII current meter*) deployed next to the cable end (Coyle & KM3NeT Collaboration, 2017).

to ensure low variations of the instrumental noise floor (<5 dB) over the whole cable length (Fernández-Ruiz, Williams, et al., 2019; Lior et al., 2021; Pastor-Graells et al., 2016; Williams et al., 2019). The cable is equipped with Corning® LEAF (Large Effective Area Fiber) optic fibers with very low attenuation (<0.19 dB/km), which improves the detection range. The instrumental strain noise floor is <100 piconstrain/ \sqrt{Hz} , comparable to optimal laboratory measurements for long fibers (Fernández-Ruiz, Williams, et al., 2019; Lior et al., 2021), and, to the best of our knowledge, to the sensitivity provided by most DAS systems along fiber cables spanning less than 40 km. The pulse wavelength was set at 1,550 nm, with 100 ns width (equivalent to a spatial resolution of 10 m), 1 GHz spectral content and 50 mW peak power. The DAS strain data were sampled at a rate of 100 Hz during the first 10 days of the experiment and 500 Hz in the remaining part of the campaign. The gauge length was set at 10 m, leading to a network of 4,480 equally spaced strain sensors. To mitigate the $1/f$ noise that affects strain recordings at low frequencies f (Fernández-Ruiz, Costa, & Martins, 2019), we converted the strain data to strain rate by finite-difference time derivation. Moreover, Jousset et al. (2018) reported that high frequency signals (1–100 Hz) can be accurately analyzed from strain rate data recorded by DAS.

A range of environmental sensors are located on the Interface Instrumented Module (MII) at the end of the cable (Coyle & KM3NeT Collaboration, 2017). We will use for comparison with the DAS measurements the data recorded by an ADCP current meter, an Aquadopp DW from Nortek, located on the MII (red triangle, Figure 1b).

3. Results

3.1. Observation of Vortex-Induced Vibrations Along Hanging Cable Sections

Our DAS datasets feature quasi-harmonic oscillations of fiber strain along cable sections laid on irregular bathymetry or where suspended sections are expected (Figures 2a and 2b). These cable oscillations are a common observation in seafloor DAS recordings, and can be readily detected by three distinguishing features of the DAS signals: (a) they have amplitudes larger than those of any other background noise, (b) they coherently extend between sharply defined points along the cable, and (c) their Fourier spectra show a characteristic frequency lower than 1 Hz, which is time-dependent. Cable oscillations can last from hours to days, separated by periods without oscillations that range from a few hours to almost half a day. Several cable segments of different lengths can vibrate simultaneously with different amplitudes. Hence, we analyze hour-long DAS recordings to identify cable segments presenting the three features previously described.

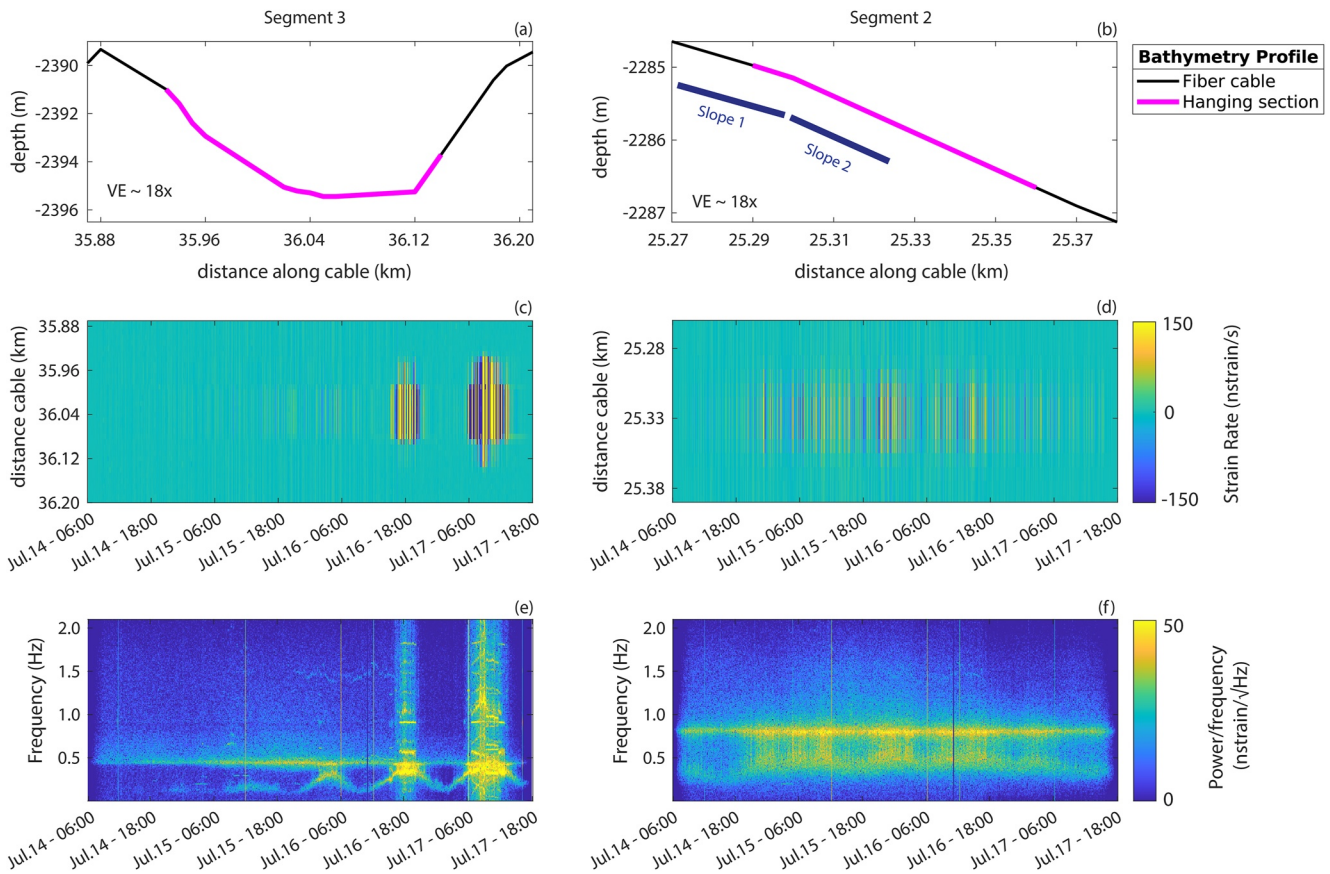


Figure 2. Vortex-induced vibrations (VIV) recorded by seafloor distributed acoustic sensing (DAS). We show two examples, in segments 3 (left) and 2 (right). (a) Bathymetry profile along the cable path (VE stands for Vertical Exaggeration) and (c) 84 hr-long recording of low-pass filtered strain rate, along a portion of Segment 3. A cutoff frequency of 2 Hz is used to filter the strain rate. Uniform quasi-harmonic oscillations of fiber strain occur around a seafloor valley. (e) Spectrogram of strain rate at the center of the vibrating section featuring a time-dependent characteristic frequency, varying from 0.1 to 0.4 Hz, and the second-order pressure peak caused by sea surface waves near 0.5 Hz (Sladen et al., 2019). Higher harmonic frequencies of VIV are excited during two periods in 16 and 17 July, accompanied by large strain amplitudes. (b, d, and f) Same as a, c, and e, but for a cable section laid across a change of seafloor slope (thick blue lines in b), in Segment 2.

Quasi-harmonic oscillations are easily recognized along the MEUST cable. We observe them along three segments located at different depths (Figure 1b). We focus here on two cable portions in segments labeled as 3 and 2 in Figure 1, since they display fundamental frequencies that extend during days and harmonics are barely observed (Figures 2c and 2d; Figure S1 in Supporting Information S1 shows oscillations of a cable section along the segment labeled as 1 in Figure 1). These cable sections span 210 and 70 m, respectively, they are 10 km apart and their depth differs by less than 120 m (Figures 2a and 2b, magenta line). The former crosses a deep ocean valley (segment 3) and the latter a change of the seafloor slope (segment 2). Both cable portions oscillate at the same time between 14 July at 06:00 and 17 July at 18:00. Between July 16th at 18:00 and July 17th at 18:00, the cable oscillations in segment 3 have amplitudes ranging from 600 to 2,300 nstrain/s, one to two orders of magnitude larger than the background noise recorded by DAS. During the same period, the amplitudes of the cable oscillations along segment 2 remain between 10 and 15 nstrain/s, slightly above the background noise. The oscillations of both cable portions have a characteristic frequency lower than 1 Hz, which fluctuates through time (Figures 2e and 2f). Harmonics are identified in segment 3, when the strain rate amplitude reaches its maximum between 14 July 06:00 and 17 July 18:00 (Figures 2e and 2f).

The origin of the cable oscillations is explained by comparing their signal properties with experimental observations of VIV. We analyze 14.5 days of fiber cable oscillations detected between 12 July at 02:10:26 and 29 July at 23:31:28 along cable segment 3 in Figure 2a. The fundamental frequency of the oscillations was present during several days in this cable portion, and harmonics were barely observed. We use two-minutes-long sliding windows to extract both the maximum absolute value of the fiber strain rate at the center of segment 3, and the

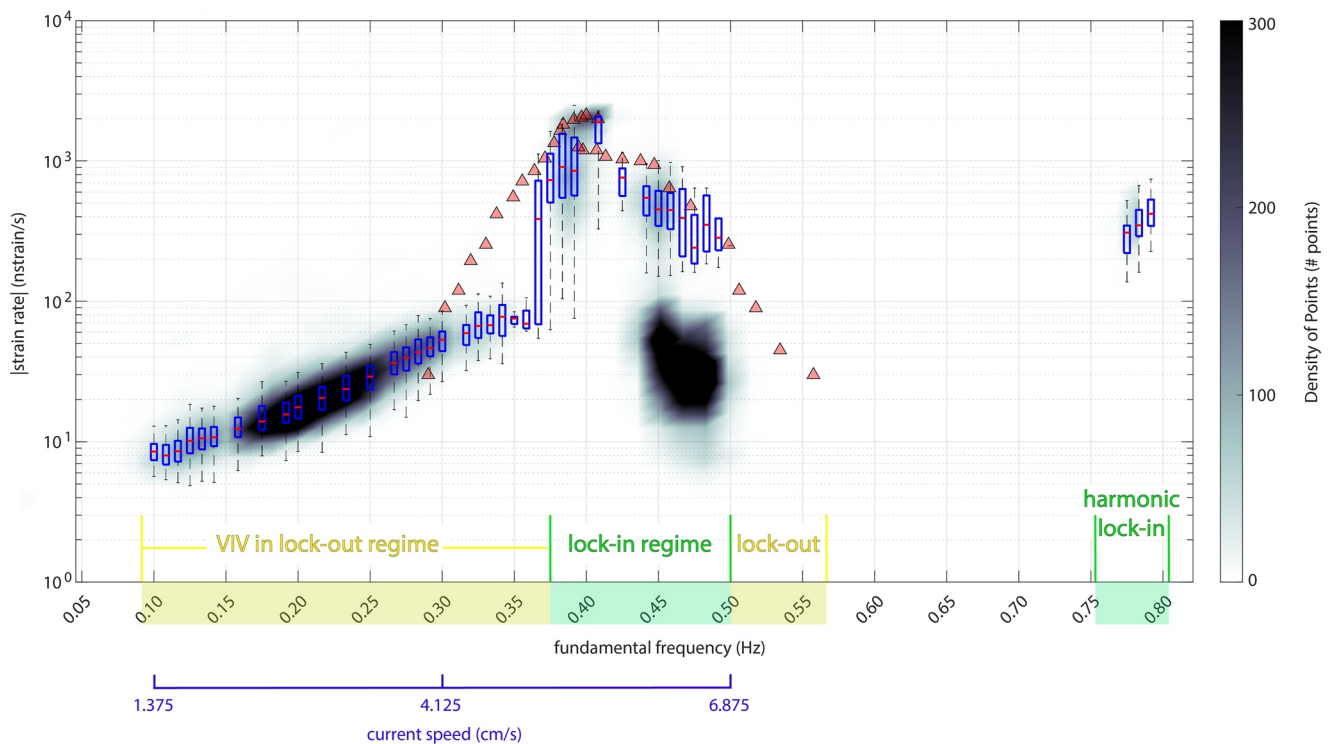


Figure 3. Evidence of vortex-induced vibrations (VIV) on a suspended underwater cable. Maximum absolute value of the fiber strain rate at the center of segment 3, during 14.5 days, over 2-min-long sliding windows, plotted as a function of the dominant frequency of the fiber oscillations (density of points). Each blue box represents the median fiber strain (red), its 25th and 75th percentiles (bottom and top edges) by frequency, respectively. The whiskers extend to the most extreme data points that are not considered outliers (dashed black lines). The amplitude increases exponentially up to a frequency close to 0.35 Hz, then more steeply as the frequency approaches 0.40 Hz. Considering that VIV frequencies are linearly related to current speeds through the Strouhal relation (blue horizontal scale), this behavior is consistent with that observed in controlled VIV experiments (triangles: experimental data of Feng, 1968, rescaled in amplitude and frequency to match the peak of the DAS data). A harmonic excited during the lock-in regime of VIV is seen around 0.79 Hz. Box-and-whiskers are not represented for the low-amplitude cluster at 0.45–0.50 Hz, which is associated with the second-order pressure peak caused by sea surface waves (the persistent peak in Figure 2e).

frequency corresponding to the maximum amplitude of the Fourier spectrum of each window. The amplitude of the cable oscillations changes systematically as a function of the changing frequency. The maximum absolute value of the fiber strain rate increases exponentially with increasing dominant frequency, up to approximately 0.35 Hz (Figure 3). From 0.35 to 0.40 Hz, the amplitude increases more steeply, then reaches a maximum. Similarly, published experimental results on VIV show that the amplitude of oscillations increases with the frequency at which vortices shed off from elongated structures (Bourguet et al., 2015; Feng, 1968; King, 1977). This frequency, also known as the vortex shedding frequency, describes the periodic pattern of the wake formed when a fluid—commonly wind in VIV experiments—flows about a stationary and slender object (King, 1977). The steepening of the VIV amplitude growth before reaching the maximum amplitude is also observed in experiments (Feng, 1968). The similarity of the amplitude versus frequency relation between the cable oscillations and that reported in the literature on VIV suggests that the characteristic oscillations recorded by seafloor DAS along segment 3 are indeed VIV of the cable induced by deep ocean currents.

Suspended sections of seafloor fiber cables can be identified through DAS recordings of VIV. To trigger VIV along underwater fibers, seafloor ocean currents must interact with hanging sections of the cable. Hence, the vortex-induced cable oscillations presented here may be used to identify spatial variations in the mechanical coupling between the cable and the seafloor. Particularly, we propose the detection of suspended underwater fiber sections by monitoring the amplitude of strain rate recorded by DAS and its standard deviation along the entire cable, as suggested by Mata Flores et al. (2023). We notice that the amplitude of the fiber strain recorded by DAS along a cable segment undergoing VIV is usually one to two orders of magnitude larger than the ambient noise recorded by the same cable section outside periods of VIV, which may be used by threshold detectors to readily pinpoint hanging sections of seafloor fibers. We observe that the amplitude of vortex-induced cable oscillations recorded by DAS decreases more than 50% along two or three consecutive channels (Figure S3 in Supporting

Information S1). Therefore, the accuracy of the suspended cable length is defined by the gauge length of the experiment. Outside periods of VIV, we did not observe a difference in the amplitude of fiber strain recorded by DAS along cable segments expected to be well coupled to the seafloor, and along nearby cable sections expected to be hanging. Mata Flores et al. (2023) reported identical results, after tracking the amplitude of DAS-recorded strain rate along an underwater fiber cable spanning 26 km. This similar amplitude of fiber strain could indicate that background noise recorded by DAS is mainly dominated by instrumental noise, regardless of the mechanical coupling between the cable and the seafloor. Alternatively, it could reveal that cable segments are not suspended when VIV is not recorded by DAS.

A persistent signal with stationary frequency is also observed along cable sections undergoing VIV, which we associate with sea surface gravity waves. Between 14 July at 06:00 and 17 July at 18:00, a frequency permanently excited can be identified in Figures 2e and 2f. This frequency is about 0.4 and 0.8 Hz in the cable sections located at segments 3 and 2, respectively. This frequency has been previously reported as featuring water-depth dependence and being related to second-order pressure fluctuations caused by sea surface gravity waves, which are at the origin of secondary microseism (Guerin et al., 2022; Sladen et al., 2019). This signal has a clear and persistent signature and does not interfere with the analysis of the oceanic VIV.

3.2. Current Speed Monitoring in Deep Ocean Environments

Cable oscillations caused by VIV are expected to have frequencies proportional to ocean current speeds, as long as the vortex shedding frequency is not close to the natural vibration frequency of the suspended cable segment. Vortex shedding frequencies near or equal to one of the natural frequencies of the hanging section may trigger a vibration of the cable in resonance, a phenomenon called “lock-in” (Worzyk, 2009). The effect of lock-in on cable oscillations recorded by DAS is discussed in the next section. Out of the lock-in regime, the cable oscillations are synchronized with the vortex shedding frequency (f_{vs}) (Bourguet & Triantafyllou, 2015), which is related to the ocean current speed normal to the cable axis (U_c) through the Strouhal number (S_t) equation:

$$f_{vs} = S_t \frac{U_c}{D} \quad (1)$$

Given S_t and the diameter of the cable (D), ocean current speeds can be estimated using Equation 1 from the vortex shedding frequencies extracted from DAS data. The Strouhal number can be taken as 0.2 for seafloor cables and relevant current conditions (Worzyk, 2009). Experimental observations indicate that in the range of Reynolds numbers (R_e), $5 \cdot 10^2 < R_e < 5 \cdot 10^5$, S_t remains around 0.2 (Bai & Alam, 2018; Katopodes, 2019). Numerical modeling of oceanic flows at basin scales commonly assumes R_e around 10^2 (Jiménez et al., 2008; Lin & Dietrich, 1994), although R_e values can exceed 10^4 in the ocean (Katopodes, 2019; Thorpe et al., 2007; Özgökmen et al., 2009).

Here, we validate the proposed VIV speed-meter concept by comparing the ocean current speeds derived from vibration frequencies recorded by DAS to those independently recorded by the nearby current meter (station MII). We focus on the vibrating cable section in segment 3 in Figure 2a, which is the closest to the current meter (3.75 km away) and is located at a similar depth (2,390 m). The corresponding DAS data are low-pass filtered below 0.35 Hz to avoid the second-order pressure peak (near 0.5 Hz, Figure 2e) and the observed lock-in frequency around 0.4 Hz (Figure 3). We picked a value of f_{vs} at every minute, as the frequency corresponding to the maximum amplitude of the Fourier spectra over 2-min sliding windows with 1-min overlap. Using Equation 1 and the cable diameter of 2.75 cm, we derive a time series of ocean current speeds from the time series of f_{vs} , with resulting values ranging from 1.11 to 5.45 cm/s (Figure 4a). The DAS-derived time series displays the component of ocean current speed normal to the cable axis hitting the cable. We assume that the incidence angle of ocean currents relative to the plane perpendicular to the cable axis is smaller than 60° , which allows using Equation 1 for oblique ocean currents (Bourguet et al., 2015). The impact of larger incidence angles on DAS-derived ocean current speeds is discussed in Section 3.4. The precision of our current speed estimates, ΔU , is controlled by the window size, $T_{window} = 120$ s, of the Fourier spectral analysis: $\Delta U = \frac{D}{S_t \cdot T_{window}} \approx 1$ mm/s. We compare the resulting DAS-derived time series to the current meter time series smoothed with a 2-hr sliding median (Figure 4a). The available data of the MII current meter indicates the positive value of the ocean current speeds and their direction. Before 27 July, the two time series agree well during periods without data gaps. Afterward, the DAS-derived current speeds are lower by more than 1 cm/s than the speeds recorded by the current

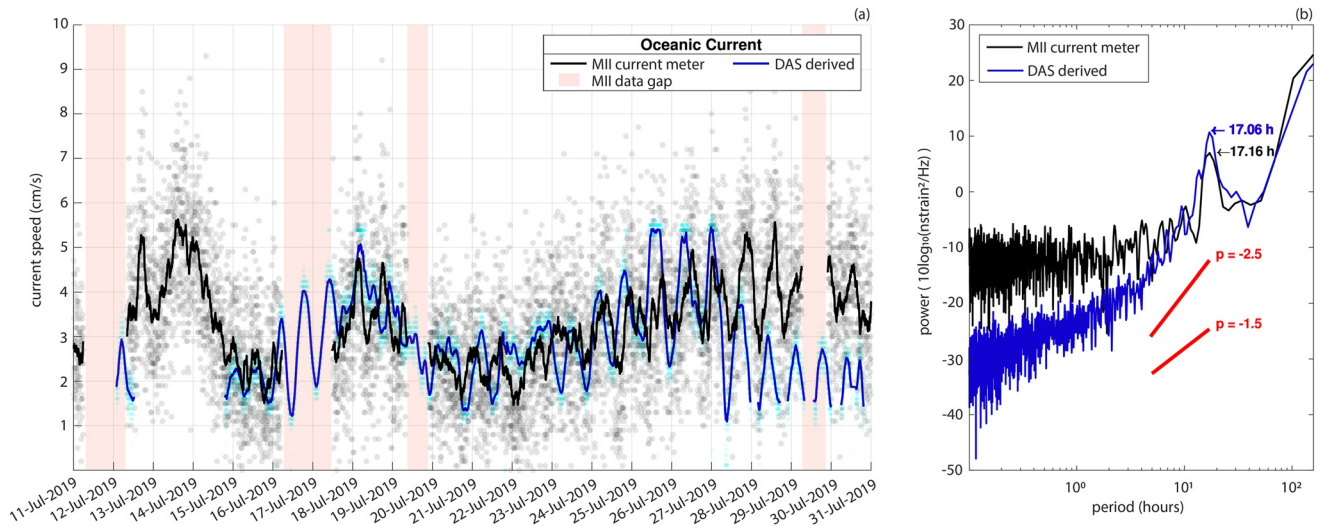


Figure 4. Deep ocean currents sensed by distributed acoustic sensing (DAS) compared to MII current meter records. (a) Ocean current speed recorded by MII current meter between 11 July 2019 00:00:00 UTC and 31 July 2019 00:00:00 UTC (gray circles), current speed derived from Strouhal frequencies sensed by DAS in a hanging section between km 37.06 and 37.18 (cyan circles) and its median over 2-hr-long sliding windows (black curve), current speed derived from Strouhal frequencies sensed by DAS in a hanging section between km 37.06 and 37.18 (cyan circles) and its median over 2-hr-long sliding windows (blue line). Pink rectangles correspond to data gaps of the MII current meter. (b) Power Spectral Density of raw MII (black) and DAS (blue) oceanic current speeds from 19 July 2019 22:09:04 to 29 July 2019 06:14:45. A 17-hr peak is observed in both spectra. The energy power of the DAS spectrum ($P(f)$) decays with increasing frequency from a period $T < 17$ hr to $T = 4$ hr following $P(f) \approx 1/f^p$, with $p = 2.5$. For reference, the red lines show the spectral decay slope for two values of the decay exponent “ p .”

meter. This deviation may be due to local perturbations affecting the ocean current speeds or their direction in the vicinity of the cable (different seafloor features, local turbulence). We further observe that the DAS-derived and current meter speeds share a common dominant period near 17 hr (see the spectral peak in Figure 4b). The implications of this detected dominant period are discussed in Section 3.5. Figure 5 shows both time series low-pass filtered with a cutoff frequency $f_{cutoff} = (10 \text{ hr})^{-1}$, to focus on the dominant period. A time-dependent time-shift is

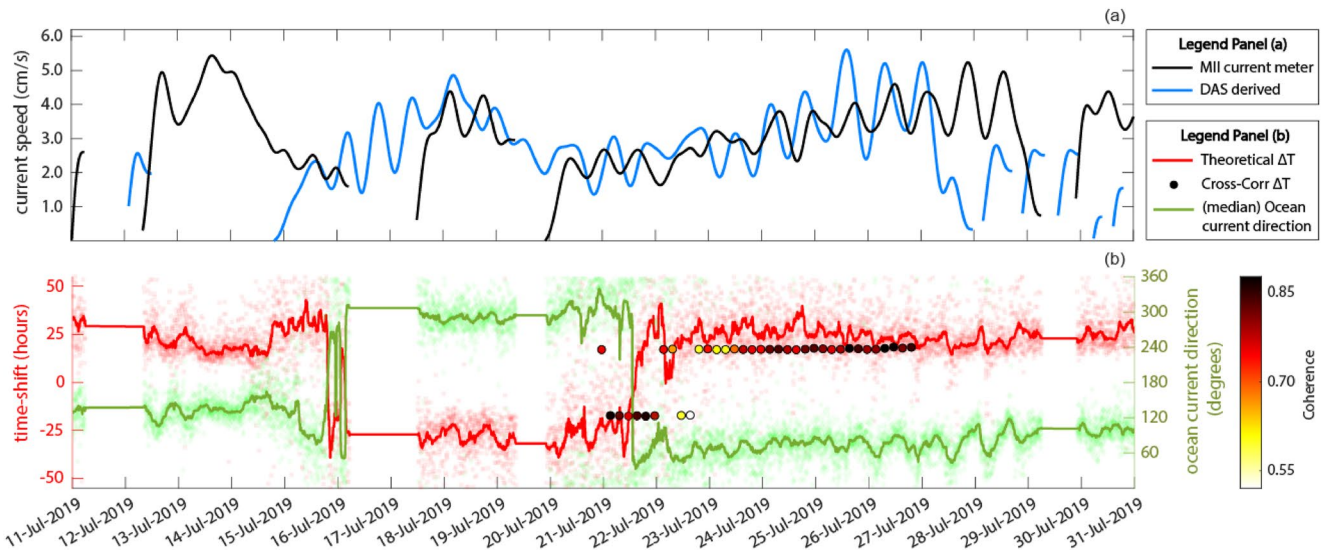


Figure 5. Impact of the ocean dynamics on current speeds measured by distributed acoustic sensing (DAS). (a) Low-pass filtered ocean current speeds: recorded by the current meter (black) and DAS-derived from the same cable section as in Figure 4 (blue), from 11 July to 31 July 2019. We low-pass filtered both time series with a cutoff period of 10 hr. (b) Expected time-shift between ocean current speeds at the MII current meter location and along the hanging cable section (red squares), derived from MII current meter data. The red line is the median expected time-shift averaged over a 2-hr sliding window. Circles: time-shift calculated by cross-correlation between MII current meter and DAS time series over a 50-hr sliding window, only shown for windows without data gaps. Coherence is shown in color scale. Ocean current direction recorded by the current meter ($\phi_{current}$, green squares). The green line is the median- $\phi_{current}$ averaged over 2-hr-long sliding windows. The time-shift sign fluctuates according to whether oceanic currents are measured first by MII current meter (negative) or by DAS (positive).

clearly observed between the two low-pass filtered time series, as expected for oceanic currents measured several kilometers away (Figure 5a). We measure the time-dependent time-shift by cross-correlation over 50-hr-long sliding windows between 20 July and 27 July, a period with no data gaps (Figure 5b). We compare it with an expected time-shift derived from:

$$\Delta T = \frac{\Delta X}{U} \cdot \cos \alpha \quad (2)$$

where $\Delta X \sim 3.75$ km is the distance between the current meter and the selected cable section, U the ocean current speed, and α the smallest angle between the cable azimuth ($\phi_{cable} = 101^\circ$) and the azimuth of the ocean current direction ($\phi_{current}$). Both U and $\phi_{current}$ were recorded by the current meter. The measured and expected time-shifts agree during periods when the ocean current features a dominant orientation (Figure 5b). Between 21 and 22 July the current meter recordings show a change of the ocean current orientation, which corresponds to a decrease in the coherence between the time series from 22 to 23 July.

3.3. Limitations Imposed by the Lock-In Regime

Oscillation frequencies recorded during lock-in, that is, while the cable vibration is in resonance with vortex shedding, cannot be readily exploited to estimate ocean current speeds. Lock-in involves large-amplitude excitation of the natural frequencies of the cable (Bourquet et al., 2015; Feng, 1968). The cable vibration frequency is then no longer controlled by the Strouhal number relation, Equation 1, but by the cable resonance frequency. Stähler et al. (2018) observed harmonic signals (fundamental and overtones) in OBS recordings at 20 m depth in the Baltic Sea, and associated them to lock-in generated by ocean currents strumming the head-buoy cable of the OBS. The multiple harmonics observed in Figure 2e in 16 July at 18:00 and in 17 July between 06:00 and 18:00, suggest VIV is operating in the lock-in regime during these time periods. We rarely observe such higher-harmonics in the DAS data recorded in segment 3. Therefore, we consider the lock-in regime does not dominate the VIV along this cable section. We propose to identify periods of lock-in by the presence of harmonics in the Fourier spectra of cable segments featuring vortex-induced cable oscillations recorded by DAS.

Lock-in imposes an upper bound on the current speed that can be estimated by VIV on DAS data. The natural frequencies (f_n) of a hanging cable portion depend on its span length (l), mass per unit length (m) and horizontal tension (T) as $f_n = \frac{n}{2l} \sqrt{\frac{T}{m}}$, where n is an integer (Irvine & Caughey, 1974). The maximum amplitude of the ocean current speed that can be constrained before lock-in emerges, that is, that satisfies the condition $f_{vs} < f_1$, is:

$$U_{\max} = \frac{D}{2S_t} \sqrt{\frac{T}{m}} \frac{1}{l} \quad (3)$$

More precisely, lock-in occurs over a range of frequencies around f_1 , roughly from $0.94f_1$ to $1.25f_1$ in the experiments reported by Feng (1968). In principle, current speeds could also be measured if they are above the lock-in range associated to f_1 , that is, above $\sim 1.25f_1$. However, the sequence of lock-in ranges related to the higher modes f_n would make this impractical. Thus, in practice Equation 3 gives the maximum current speed that can be measured by our proposed method.

The maximum measurable speed can be estimated from known cable properties. Using the relation $T = \frac{mgl^2}{8d}$ (Irvine & Caughey, 1974), where g is the gravitational acceleration and d the sag of the cable, Equation 3 becomes:

$$U_{\max} = \frac{D\sqrt{2g}}{8S_t} \frac{1}{d^{1/2}} \quad (4)$$

If $d/l \leq 1/8$, as expected in submarine cables, the sag d is related to the curvilinear length of the suspended cable by $L \approx l \left[1 + \frac{8}{3} \left(\frac{d}{l} \right)^2 \right]$ (Irvine & Caughey, 1974). We further assume that length L and span l are related by a cable layout parameter: the slack reported during the cable deployment, $S = L/l - 1 \approx \frac{8}{3} \left(\frac{d}{l} \right)^2$ (Abidin et al., 2018). We then obtain:

$$U_{\max} = \frac{A_n}{l^{1/2}} \quad (5)$$

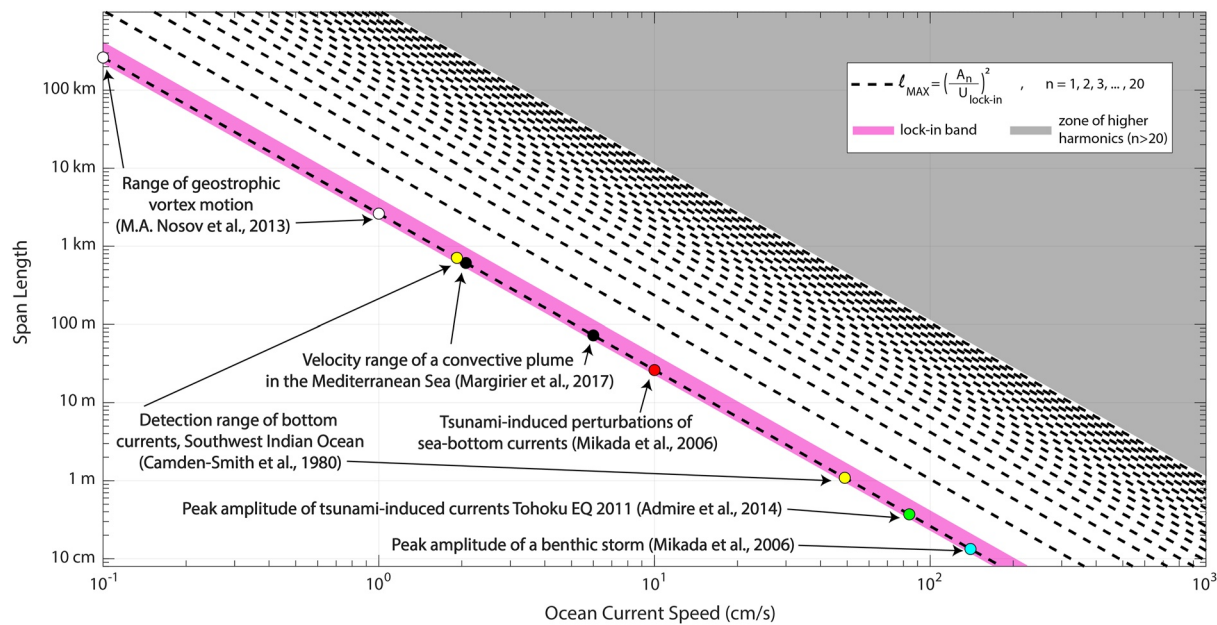


Figure 6. Permissible range of suspended cable span lengths and current speeds imposed by the lock-in condition in the Mediterranean Eurocentre for Underwater Sciences and Technologies cable. Maximum span lengths are shown as a function of expected peak current speeds detected by DAS, together with the lock-in range reported by Feng (1968) (black lines and pink rectangle, respectively). Adjusting the span length of a suspended section in cable segment 3, from kilometers-long to centimeters-long, may allow detecting peak current speeds associated to several processes in oceanography (circles).

where $A_n = nA_1$ and

$$A_1 = \frac{D\sqrt{2g}\sqrt[4]{24S}}{24S S_t} \quad (6)$$

Equation 5 provides an estimate of the largest current speed accessible with a given span length l of suspended cable, given two geometrical parameters of the cable, its diameter D and its slack S . Conversely, it provides the longest suspended cable span length, $l_{\max} = (A_n/U_{\max})^2$, that can be utilized to monitor seafloor current speeds up to a given target value U_{\max} .

According to Equation 5 detecting faster currents requires shorter suspended cable sections. Figure 6 displays the permissible range of span lengths and current speeds in the MEUST cable, assuming the same values of D and S_t as for Equation 1. The peak current speeds reached by various oceanography processes are also indicated in Figure 6. Considering suspended cable sections of different lengths, DAS observations should allow to monitor a wide range of oceanography processes: tsunami-induced geostrophic vortices (Nosov et al., 2013) using kilometers-long cable spans, sea-bottom currents, convective plumes motion and tsunami-induced perturbations (Camden-Smith et al., 1981; Margirier et al., 2017; Mikada et al., 2006) with meters-long cable spans, turbidity currents, such as benthic storms and tsunami-induced currents (Admire et al., 2014; Mikada et al., 2006), using centimeters-long cable spans. More DAS campaigns are needed to validate the capability of the VIV-speedmeter method to properly monitor this wide spectrum of oceanography processes. Special care must be taken to study oceanic processes featuring slow current speeds, since they should generate smaller VIV-amplitudes detected by DAS along shorter suspended cable sections.

3.4. VIV Under Oblique Seafloor Currents

Under certain conditions, Equation 1 is expected to be valid also when the current hits the cable obliquely, if U_c is defined as the cable-normal component of the current speed, that is, the projection of the current speed vector onto the plane perpendicular to the cable axis. The literature on oblique-VIV commonly examines the accuracy of attributing VIV frequencies and flow dynamics to the component of the current speed perpendicular to the axis of the oscillating body (Bourguet et al., 2015). The so-called Independence Principle (IP) or cosine law

postulates that the physical quantities of oblique and normal VIV (fluid forces, vortex shedding, vibration amplitudes) should match if the normal component of the current speed is the same (Bourguet et al., 2015). Numerical simulations show that the IP is valid as long as the incidence angle relative to the plane perpendicular to the cable axis is smaller than 60° (Bourguet et al., 2015).

To investigate this Independence Principle, we compare the cable-normal component of the current meter speed to the DAS-derived time series. To do so, we calculate the angle θ between the ocean current direction recorded by the current meter and the plane perpendicular to the cable. We then compute the cable-normal component of the current meter speed ($U_{MI} \cdot \cos(\theta)$) and compare it to the DAS-derived speed (U_{DAS}) (Figure S2 in Supporting Information S1). The resulting time series are not in agreement ($U_{MI} \cdot \cos(\theta) \neq U_{DAS}$), which does not support the IP. We cannot attribute this negative result to the validity range of θ : the IP is expected to fail if $\theta > 60^\circ$ (Bourguet et al., 2015; Bourguet & Triantafyllou, 2015; Lucor & Karniadakis, 2003), but here θ ranges from 24 to 82° . Our negative result could be biased by the high variability of θ , and the non-negligible distance between the cable and the reference current meter (3.75 km). Dedicated instrument deployment is therefore needed to study the limitations of the IP in predicting physical quantities of oblique VIV recorded by DAS.

3.5. Observing Internal Gravity Waves in the Mediterranean Sea

Spectral analysis of DAS-derived ocean current speed time series provides quantitative information about internal gravity waves generated in the Mediterranean Sea. The Power Spectral Density estimates (PSD's) of DAS-derived and current meter speed time series between 19 July at 22:09:04 and 29 July at 06:14:45 show a strong peak around a period of 17 hr (Figure 4b). This peak has been previously observed in ocean current speed time series recorded in the Mediterranean Sea (Van Haren & Millot, 2003). It has been associated with near-inertial waves generated in the Mediterranean basin during summer, that is, internal gravity waves with periods close to the so-called local inertial period ($T_{inertial}$), which is primarily controlled by Earth's rotation rate ($\Omega \sim 2\pi/24$ hr) and location latitude (φ). The theoretical value at the current meter location ($\varphi = 42.805^\circ$) is $T_{inertial} = 2\pi/f_{coriolis} = 17.66$ hr, using the Coriolis frequency (Van Haren & Millot, 2003):

$$f_{coriolis} = 2 \Omega \sin \varphi \quad (7)$$

The difference of 0.60 μHz between our theoretical and observed frequencies is smaller than the uncertainty in our determination of the observed frequency, which is given by the frequency sampling of our PSD's, 1.75 μHz (based on of 158 hr-long sliding windows).

The spectrum of the DAS-derived speed decays in a way consistent with ocean stratification processes. Between $T < 17$ hr and $T \approx 4.02$ hr it decays as $P(f) \approx 1/f^{2.5}$ (Figure 4b). This is consistent with the weak turbulence theory that predicts a variety of power laws for the energy spectrum of internal gravity waves generated in the ocean (Garrett & Munk, 1979; Lvov et al., 2010). Previous observations by Van Haren and Millot (2003) show that the kinetic-energy spectra of near-inertial waves decay as $P(f) \approx 1/f^p$, with p a seasonal parameter that fluctuates between 1.5 and 2.5 during summer in the Mediterranean sea. According to Van Haren and Millot (2003), the seasonal variation of the ocean stratification is the process at the origin of the fluctuations of the p value. The DAS-derived current speed spectrum over longer times should be able to capture the seasonal variation of p , which can offer novel opportunities to monitor the dynamics of ocean stratification. The permissible frequency range of internal gravity waves is $f_{coriolis} < f < N$, with N the Buoyancy frequency that depends on the ocean depth and stratification (Garrett & Munk, 1979). Van Haren and Millot (2003) have estimated $N \approx 3f_{coriolis}$ at 1,100 m depth, from density-depth profiles recorded by moorings during summer in the Mediterranean Sea, while Van Haren (2014) suggested that deeper, around 2,200 m, $N \approx 4f_{coriolis}$. The spectrum decay of the DAS-derived current speeds detected at 2,390 m depth is described by the power law down to a period of 4.02 hr (Figure 4b), which is in agreement with the expected lower bound period $T = 4.42$ hr that results from $N \approx 4f_{coriolis}$.

4. Conclusions

We investigated the potential of DAS to monitor deep sea currents along suspended sections of underwater fiber optic cables. We demonstrated that oblique VIV can be recorded by DAS along cable sections presumably hanging due to irregular seafloor conditions. The oscillations showed time-dependent amplitudes larger than those of any other background noise and amplitude-dependent characteristic frequencies, as expected for VIV, lower than

1 Hz at different depths. We observed vortex-induced cable oscillations featuring amplitudes one to two orders of magnitude larger than the background noise recorded by DAS, which suggests these vibrations may be sensed by any DAS interrogator.

To the best of our knowledge, this is the first quantitative analysis of seafloor circulation using DAS data along hanging cable sections. The measured ocean currents speed recovered in this study ranged from 1.11 to 5.45 cm/s and matched those of a current meter located 3.75 km away but at a similar depth. Both time series showed a similar dominant period and correlation after time shift. The DAS-derived current speed time series displays features, such as characteristic periods and spectral decay, associated with known oceanographic processes: the generation of internal gravity waves and weak turbulence. Thus, DAS offers novel opportunities to monitor oceanographic processes at depths barely studied with the current instrumentation.

Our estimates of current speeds from vortex shedding frequencies recorded by DAS were derived through the Strouhal number equation. This approach is valid in the range of Reynolds numbers where the Strouhal constant remains close to 0.2. Since vortex shedding frequencies close to lock-in are not described by the Strouhal relation, we limited our analysis to conditions where the lock-in frequency is the upper limit of the method. The possibility to monitor the currents beyond the lock-in frequency is left for further studies. Also, more experiments are still needed to determine the lower limit of ocean current speeds that DAS is able to record, and if the Independence Principle holds for small incidence angles of the current on the cable.

The DAS-based monitoring of deep ocean currents presented here may be useful to investigate a variety of oceanography processes. We suggest to perform DAS experiments along controlled sections of suspended underwater cables, to validate the contribution of DAS-recorded VIV in the monitoring of several submarine processes. If the cable used in this study had nearby hanging cable segments with different orientations, we hypothesize that they could be used as an antenna to track changes in orientation of the ocean circulation.

Data Availability Statement

The fiber optic DAS datasets used to generate Figures 2–5 and Figures S1–S3 in Supporting Information S1 are available in the following OSF repository: <https://osf.io/cfwb3/> (Mata Flores, 2022).

Acknowledgments

We thank the two anonymous reviewers that allowed us to improve our work with their constructive comments. The work of D.M.F. was funded by a joint fellowship of the Observatory of Côte d'Azur (OCA) and Region Sud. The MEUST-NUMer-Env project is sponsored by CNRSIN2P3, the Region Sud, France (CPER), the State (DRRT), and the Europe (FEDER). This work was partially supported by the SEAFOOD project, funded by grant ANR-17-CE04-0007 of the French Agence Nationale de la Recherche and the Doelbin Federation (FR2800 CNRS).

References

- Abidin, A. R. Z., Mustafa, S., Aziz, Z. A., & Ismail, K. (2018). Subsea cable laying problem. *MATEMATIKA: Malaysian Journal of Industrial and Applied Mathematics*, 34(2), 173–186. <https://doi.org/10.11113/matematika.v34.n2.1064>
- Admiral, A. R., Dengler, L. A., Crawford, G. B., Uslu, B. U., Borrero, J. C., Greer, S. D., & Wilson, R. I. (2014). Observed and modeled currents from the Tohoku-Oki, Japan and other recent tsunamis in northern California. *Pure and Applied Geophysics*, 171(12), 3385–3403. <https://doi.org/10.1007/s00024-014-0797-8>
- Bai, H., & Alam, M. M. (2018). Dependence of square cylinder wake on Reynolds number. *Physics of Fluids*, 30(1), 015102. <https://doi.org/10.1063/1.4996945>
- Bourguet, R., Karniadakis, G. E., & Triantafyllou, M. S. (2015). On the validity of the independence principle applied to the vortex-induced vibrations of a flexible cylinder inclined at 60°. *Journal of Fluids and Structures*, 53, 58–69. <https://doi.org/10.1016/j.jfluidstructs.2014.09.005>
- Bourguet, R., & Triantafyllou, M. S. (2015). Vortex-induced vibrations of a flexible cylinder at large inclination angle. *Philosophical Transactions of the Royal Society A: Mathematical, Physical & Engineering Sciences*, 373(2033), 20140108. <https://doi.org/10.1098/rsta.2014.0108>
- Bryden, H. L., Robinson, C., & Griffiths, G. (2012). Changing currents: A strategy for understanding and predicting the changing ocean circulation. *Philosophical Transactions of the Royal Society A: Mathematical, Physical & Engineering Sciences*, 370(1980), 5461–5479. <https://doi.org/10.1098/rsta.2012.0397>
- Camden-Smith, F., Perrins, L.-A., Dingle, R., & Brundrit, G. (1981). A preliminary report on long-term bottom-current measurements and sediment transport/erosion in the Agulhas passage, southwest Indian Ocean. *Marine Geology*, 39(3–4), M81–M88. [https://doi.org/10.1016/0025-3227\(81\)90069-4](https://doi.org/10.1016/0025-3227(81)90069-4)
- Coyle, P., & KM3NeT Collaboration. (2017). KM3NeT-ORCA: Oscillation research with cosmics in the abyss. *Journal of Physics: Conference Series*, 888, 012024. <https://doi.org/10.1088/1742-6596/888/1/012024>
- Duennebie, F. K., Blackinton, G., & Sutton, G. H. (1981). Current-generated noise recorded on ocean bottom seismometers. *Marine Geophysical Researches*, 5(1), 109–115. <https://doi.org/10.1007/bf00310316>
- Feng, C. (1968). *The measurement of vortex induced effects in flow past stationary and oscillating circular and d-section cylinders (Unpublished doctoral dissertation)*. University of British Columbia.
- Fernández-Ruiz, M. R., Costa, L., & Martins, H. (2019). Distributed acoustic sensing using chirped-pulse phase-sensitive OTDR technology. *Sensors*, 19(20), 4368. <https://doi.org/10.3390/s19204368>
- Fernández-Ruiz, M. R., Williams, E. L., Magalhaes, R., Vanthillo, R., Costa, L., Zhan, Z., et al. (2019). Teleseisms monitoring using chirped-pulse ϕ OTDR. *Seventh European workshop on optical fibre sensors*, 11199, 1119921.
- Garrett, C., & Munk, W. (1979). Internal waves in the ocean. *Annual Review of Fluid Mechanics*, 11(1), 339–369. <https://doi.org/10.1146/annurev.fl.11.010179.002011>
- Guerin, G., Rivet, D., van den Ende, M., Stutzmann, E., Sladen, A., & Ampuero, J. (2022). Quantifying microseismic noise generation from coastal reflection of gravity waves recorded by seafloor das. *Geophysical Journal International*, 231(1), 394–407. <https://doi.org/10.1093/gji/ggac200>

- Hartog, A. H. (2017). *An introduction to distributed optical fibre sensors*. CRC press.
- Hong, K.-S., & Shah, U. H. (2018). Vortex-induced vibrations and control of marine risers: A review. *Ocean Engineering*, *152*, 300–315. <https://doi.org/10.1016/j.oceaneng.2018.01.086>
- Howe, B. M., Arbic, B. K., Aucan, J., Barnes, C. R., Bayliff, N., Becker, N., et al. (2019). Smart cables for observing the global ocean: Science and implementation. *Frontiers in Marine Science*, *6*, 424. <https://doi.org/10.3389/fmars.2019.00424>
- Irvine, H. M., & Caughey, T. K. (1974). The linear theory of free vibrations of a suspended cable. *Proceedings of the Royal Society of London. A. Mathematical and Physical Sciences*, *341*(1626), 299–315.
- Jiménez, B., Sangrà, P., & Mason, E. (2008). A numerical study of the relative importance of wind and topographic forcing on oceanic eddy shedding by tall, deep water islands. *Ocean Modelling*, *22*(3–4), 146–157. <https://doi.org/10.1016/j.ocemod.2008.02.004>
- Jousset, P., Reinsch, T., Ryberg, T., Blanck, H., Clarke, A., Aghayev, R., et al. (2018). Dynamic strain determination using fibre-optic cables allows imaging of seismological and structural features. *Nature Communications*, *9*(1), 2509. <https://doi.org/10.1038/s41467-018-04860-y>
- Katopodes, N. D. (2019). Viscous fluid flow. In *Free-surface flow* (pp. 324–426). Butterworth-Heinemann.
- King, R. (1977). A review of vortex shedding research and its application. *Ocean Engineering*, *4*(3), 141–171. [https://doi.org/10.1016/0029-8018\(77\)90002-6](https://doi.org/10.1016/0029-8018(77)90002-6)
- Lamare, P. (2016). The MEUST deep sea infrastructure in the Toulon site. *EPJ Web of Conferences*, *116*, 09001. <https://doi.org/10.1051/epjconf/201611609001>
- Lin, C. A., & Dietrich, D. (1994). A numerical study of low Reynolds number 2-dimensional convective adjustment. *Geophysical and Astrophysical Fluid Dynamics*, *74*(1–4), 123–134. <https://doi.org/10.1080/03091929408203635>
- Lindsey, N. J., Dawe, T. C., & Ajo-Franklin, J. B. (2019). Illuminating seafloor faults and ocean dynamics with dark fiber distributed acoustic sensing. *Science*, *366*(6469), 1103–1107. <https://doi.org/10.1126/science.aay5881>
- Lior, I., Sladen, A., Rivet, D., Ampuero, J.-P., Hello, Y., Becerril, C., et al. (2021). On the detection capabilities of underwater distributed acoustic sensing. *Journal of Geophysical Research: Solid Earth*, *126*(3), e2020JB020925. <https://doi.org/10.1029/2020jb020925>
- Lucor, D., & Karniadakis, G. E. (2003). Effects of oblique inflow in vortex-induced vibrations. *Flow, Turbulence and Combustion*, *71*(1), 375–389. <https://doi.org/10.1023/b:appl.0000014929.90891.4d>
- Lvov, Y. V., Polzin, K. L., Tabak, E. G., & Yokoyama, N. (2010). Oceanic internal-wave field: Theory of scale-invariant spectra. *Journal of Physical Oceanography*, *40*(12), 2605–2623. <https://doi.org/10.1175/2010jpo4132.1>
- Margirier, F., Bosse, A., Testor, P., l'Hévéder, B., Mortier, L., & Smeed, D. (2017). Characterization of convective plumes associated with oceanic deep convection in the northwestern Mediterranean from high-resolution in situ data collected by gliders. *Journal of Geophysical Research: Oceans*, *122*(12), 9814–9826. <https://doi.org/10.1002/2016jc012633>
- Marra, G., Fairweather, D., Kamalov, V., Gaynor, P., Cantono, M., Mulholland, S., et al. (2022). Optical interferometry–based array of seafloor environmental sensors using a transoceanic submarine cable. *Science*, *376*(6595), 874–879. <https://doi.org/10.1126/science.abo1939>
- Mata Flores, D. (2022). Monitoring of deep sea currents with seafloor DAS [Dataset]. Open science framework. <https://doi.org/10.17605/OSF.IO/CFWB3>
- Mata Flores, D., Mercerat, E. D., Ampuero, J. P., Rivet, D., & Sladen, A. (2023). Identification of two vibration regimes of underwater fibre optic cables by Distributed Acoustic Sensing. *Geophysical Journal International*. <https://doi.org/10.1093/gji/ggad139>
- Mikada, H., Mitsuzawa, K., Matsumoto, H., Watanabe, T., Morita, S., Otsuka, R., et al. (2006). New discoveries in dynamics of an m8 earthquake-phenomena and their implications from the 2003 tokachi-oki earthquake using a long term monitoring cabled observatory. *Tectonophysics*, *426*(1–2), 95–105. <https://doi.org/10.1016/j.tecto.2006.02.021>
- Munk, W., & Wunsch, C. (1998). Abyssal recipes II: Energetics of tidal and wind mixing. *Deep Sea Research Part I: Oceanographic Research Papers*, *45*(12), 1977–2010. [https://doi.org/10.1016/s0967-0637\(98\)00070-3](https://doi.org/10.1016/s0967-0637(98)00070-3)
- Nosov, M. A., Moshenceva, A. V., & Kolesov, S. V. (2013). Horizontal motions of water in the vicinity of a tsunami source. *Pure and Applied Geophysics*, *170*(9), 1647–1660. <https://doi.org/10.1007/s00024-012-0605-2>
- Özgökmen, T. M., Iliescu, T., & Fischer, P. F. (2009). Reynolds number dependence of mixing in a lock-exchange system from direct numerical and large eddy simulations. *Ocean Modelling*, *30*(2–3), 190–206. <https://doi.org/10.1016/j.ocemod.2009.06.013>
- Pastor-Graells, J., Martins, H. F., Garcia-Ruiz, A., Martin-Lopez, S., & Gonzalez-Herraez, M. (2016). Single-shot distributed temperature and strain tracking using direct detection phase-sensitive OTDR with chirped pulses. *Optics Express*, *24*(12), 13121–13133. <https://doi.org/10.1364/oe.24.013121>
- Rahmstorf, S. (2002). Ocean circulation and climate during the past 120,000 years. *Nature*, *419*(6903), 207–214. <https://doi.org/10.1038/nature01090>
- Roemmich, D., Johnson, G. C., Riser, S., Davis, R., Gilson, J., Owens, W. B., et al. (2009). The Argo program: Observing the global ocean with profiling floats. *Oceanography*, *22*(2), 34–43. <https://doi.org/10.5670/oceanog.2009.36>
- Semtner, A. J. (1995). Modeling ocean circulation. *Science*, *269*(5229), 1379–1385. <https://doi.org/10.1126/science.269.5229.1379>
- Sladen, A., Rivet, D., Ampuero, J. P., De Barros, L., Hello, Y., Calbris, G., & Lamare, P. (2019). Distributed sensing of earthquakes and ocean-solid Earth interactions on seafloor telecom cables. *Nature Communications*, *10*(1), 5777. <https://doi.org/10.1038/s41467-019-13793-z>
- Stähler, S. C., Schmidt-Aursch, M. C., Hein, G., & Mars, R. (2018). A self-noise model for the German DEPAS OBS pool. *Seismological Research Letters*, *89*(5), 1838–1845. <https://doi.org/10.1785/0220180056>
- Thorpe, S. A. (2007). *An introduction to ocean turbulence* (Vol. 10). Cambridge University Press.
- Trim, A., Braaten, H., Lie, H., & Tognarelli, M. (2005). Experimental investigation of vortex-induced vibration of long marine risers. *Journal of Fluids and Structures*, *21*(3), 335–361. <https://doi.org/10.1016/j.jfluidstructs.2005.07.014>
- Van Haren, H. (2014). High-frequency internal wave motions at the Antares site in the deep Western Mediterranean. *Ocean Dynamics*, *64*(4), 507–517. <https://doi.org/10.1007/s10236-014-0702-0>
- Van Haren, H., & Millot, C. (2003). Seasonality of internal gravity waves kinetic energy spectra in the Ligurian basin. *Oceanologica Acta*, *26*(5–6), 635–644. [https://doi.org/10.1016/s0399-1784\(03\)00062-8](https://doi.org/10.1016/s0399-1784(03)00062-8)
- Williams, E. F., Fernández-Ruiz, M. R., Magalhaes, R., Vanthillo, R., Zhan, Z., González-Herráez, M., & Martins, H. F. (2019). Distributed sensing of microseisms and teleseisms with submarine dark fibers. *Nature Communications*, *10*(1), 5778. <https://doi.org/10.1038/s41467-019-13262-7>
- Williams, E. F., Zhan, Z., Martins, H. F., Fernandez-Ruiz, M. R., Martin-Lopez, S., Gonzalez-Herraez, M., & Callies, J. (2022). Surface gravity wave interferometry and ocean current monitoring with ocean-bottom das. *Journal of Geophysical Research: Oceans*, *127*(5), e2021JC018375. <https://doi.org/10.1029/2021jc018375>
- Worzyk, T. (2009). *Submarine power cables: Design, installation, repair, environmental aspects*. Springer Science and Business Media.

- Wunsch, C. (2016). Global ocean integrals and means, with trend implications. *Annual Review of Marine Science*, 8, 1–33. <https://doi.org/10.1146/annurev-marine-122414-034040>
- Zhan, Z., Cantono, M., Kamalov, V., Mecozzi, A., Müller, R., Yin, S., & Castellanos, J. C. (2021). Optical polarization–based seismic and water wave sensing on transoceanic cables. *Science*, 371(6532), 931–936. <https://doi.org/10.1126/science.abe6648>